

# Robust topological insulator surface conduction under strong surface disorder

Liang Du, Quansheng Wu, and Vincent E. Sacksteder IV<sup>1\*</sup>  
*Institute of Physics, Chinese Academy of Sciences, Beijing 100190, China*  
 (Dated: December 13, 2012)

Topological insulators are characterized by specially protected conduction on their outer boundaries, i.e. on their surfaces. We show that the protected surface conduction exhibited by 2-D topological insulators is independent of non-magnetic surface disorder. In particular, the surface band remains conducting even when surface state inhomogeneities destroy the characteristic linear Dirac relation between energy and momentum. The main effects of disorder are to pull the surface states into the disordered layers, decrease their Fermi velocity, and increase the density of states. These effects are controlled by a resonance between the disorder potential and the bulk bands. The resonance's energy is set by the bulk band width; protection of the Dirac cone is controlled by the bulk band width, not the bulk band gap.

PACS numbers: 72.25.-b, 73.25.+i, 72.15.Rn, 71.70.Ej

## I. INTRODUCTION

Recently a new kind of material has been predicted and measured: topological insulators, which do not permit current to flow through their interior but do allow metallic conduction along their surfaces.<sup>1-5</sup> The conducting surface states are protected topologically, meaning that they are safeguarded by the bulk's insulating property from any finite-size perturbations. The surface states obey a linear Dirac dispersion like that seen in graphene, but unlike graphene their spin degeneracy is strongly broken, the angles of the spin and the momentum are locked to each other, and  $T$  symmetry prohibits any gap in the Dirac dispersion. Topological insulators (TIs) have won tremendous theoretical and experimental interest because these special properties have potential for spintronics and quantum computation. However TIs continue to face critical experimental challenges. Chief among these are elimination of residual bulk carriers from dopants introduced by the TI growth process and by exposure to air, control of the Fermi level which responds strongly to doping, and fabrication of clean and stable surfaces.

This present article focuses on how non-magnetic disorder located *only on the TI surface* affects topological protection. Several experiments have shown that TI surface states are not destroyed even under exposure to air.<sup>6-9</sup> However three recent experiments measured the surface band while progressively doping the TI surface with impurities.<sup>10-12</sup> They saw the angularly resolved photoemission spectroscopy (ARPES) signal - an image of the Dirac cone - become progressively fainter and more blurred as impurities were added. Moreover several recent experiments have modified the TI surface by introducing an Al capping layer, or by gating the TI.<sup>13,14</sup> Another experiment reported that exposure to air causes growth of an oxide layer on top of the TI.<sup>15</sup> Therefore a better understanding is needed of surface disorder's effects on topological protection of TI surface states. In particular, we will see that direct measurements of the Dirac cone (such as ARPES and Schlubnikov-de Haas

measurements of 3-D TIs) are quite sensitive to disorder. Strong surface disorder can disrupt the Dirac cone and extinguish these experimental signals while leaving the surface conductance intact.

The current literature offers two lenses for understanding topological protection. The first lens is focused on bulk properties which protect the surface states. In TIs the bulk valence and conduction bands are split both by a strong spin-orbit interaction and by a gap whose width is controlled by a mass parameter  $m$ . If the mass and spin-orbit terms have opposite signs, the conflict between the two signs entangles the valence band with the conduction band, and the states of each band acquire a special texture centered on the  $\vec{k} = 0$   $\Gamma$  point.<sup>16</sup> This situation, called band inversion, strongly affects the TI's electronic structure both at its surfaces and also at its boundaries with any material having a positive (non-inverted) mass. On these surfaces the band inversion creates a band of surface states which connects the valence and conduction bands with each other and therefore bridges the bulk gap. If the Fermi level lies in the bulk gap, then any states in the bulk decay exponentially and current flows only in the surface states caused by the band inversion.

The surface states are safeguarded - topologically protected - by the bulk band gap. Destruction of the surface band can occur only when surface states tunnel from one side of the sample to the other, i.e. when the bulk states at the Fermi level become delocalized. Such delocalization could be caused by the sample's geometry,<sup>17,18</sup> by interactions,<sup>19</sup> or by disorder-assisted percolation through the bulk.<sup>20,21</sup> Whatever its source, bulk delocalization is not possible unless the bulk gap is destroyed throughout the sample, which is not possible with surface disorder. In particular, surface disorder leaves the bulk band gap unchanged. Therefore we should expect TI surface states to be robust against surface disorder. If the surface disorder is strong enough to locally change the band structure in the disordered region, then the TI surface states will simply detour around the disorder and ride the boundary between the disordered surface and the clean TI bulk.<sup>22,23</sup>

The second lens for understanding topological protection focuses on the surface states and their spin texture.  $T$  symmetry requires that near the  $\Gamma$  point the surface band of a topological insulator must be a linear Dirac cone, and that the angles of the spin and the momentum must be locked together. This spin texture has far reaching consequences for surface conduction both in two and in three dimensions. In a 2-D TI the Dirac cone is composed of only two edge states which have opposite spin quantum number and opposite momenta  $|\vec{p}| = \pm E_F/v_F$ , where  $E_F$  and  $v_F$  are respectively the Fermi energy and Fermi velocity. Non-magnetic disorder is unable to flip the spin and therefore leaves the edge conductance always quantized at  $2G_0$ , where  $G_0$  is the conductance quantum. In a 3-D TI the spin's effect is bit more subtle, since it permits scattering at any angle except 180 degrees. In this case spin-momentum locking implies that electrons pick up a  $\pi$  Berry phase every time that they make a closed loop. This Berry phase reverses the sign of disorder's effects on the conductance: weak disorder causes an increase in the conductance, as is typical in systems with strong spin-orbit coupling.<sup>24</sup> Non-perturbative numerical studies of purely surface conduction with a single Dirac cone surface band indicate that the conductance increases without limit, proportional to  $\ln L$  where  $L$  is the wire length.<sup>25,26</sup> This is much different from long non-topological wires, where the conductance invariably decreases to zero. These arguments based only on the Dirac cone and on spin-momentum locking give a detailed picture of how topological protection affects scattering processes.

How does topological protection work when surface disorder becomes large? Recently Schubert et al<sup>23</sup> performed a numerical simulation of 3-D TIs with surface disorder and found that the surface band evolves through three regimes when the surface disorder is increased. At small disorder the surface states are close to plane waves and follow a linear Dirac dispersion. However when the disorder grows larger the in-gap states are no longer homogenous plane waves and therefore the linear Dirac relation between momentum and energy disappears. This is consistent with several experimental studies which saw the Dirac cone weaken and blur as surface disorder was increased.<sup>10-12</sup> Lastly at very large surface disorder the in-gap states move just inside the disordered region and return to the Dirac dispersion found at weak disorder. Based on these numerical results, Schubert et al argued that when the disorder is larger than the gap the bulk and surface states mix, the Dirac cone is destroyed, and the TI surface states are no longer topologically protected.

The present paper studies the same physics, but in 2-D TIs, where the quantized  $2G_0$  conductance simplifies analysis, much larger sample sizes are accessible, and statistical errors and finite size effects are more easily controlled. We confirm that there are three disorder regimes. Like Schubert et al, we show that in the intermediate disorder regime the surface states are inhomogeneous (not plane waves) and therefore do not follow any dispersion

relation between energy and momentum. However we also show that surface conduction is topologically protected at any disorder strength - the  $2G_0$  quantization is never destroyed by surface disorder. In this intermediate disorder regime direct measurements of the energy dispersion will find no signal of the Dirac cone, while transport experiments will show robust surface conduction.

Going further, we find that the inhomogeneous states at intermediate disorder are controlled by a resonance between the disorder potential and the bulk bands. Both the resonance and the accompanying disruption of the Dirac cone occur at the characteristic energy scale of the bulk bands; the Dirac cone is protected by the bulk band width, not by the much smaller bulk band gap. The main effects of disorder in the resonant region are to pull the surface states into the disordered outer layers, increase the density of states, and decrease the Fermi velocity.

The structure of this paper is as follows. In section II we describe our model of a 2-D TI and the numerical methods which we use to study it, in section III we present and discuss our numerical results, and in section IV we discuss the interpretation and physics of these results.

## II. METHODS

We study the Bernevig-Hughes-Zhang (BHZ) tight binding model<sup>16</sup> of 2-D topological insulators. This model was obtained by starting with the six-band Kane model of the  $\Gamma_6$  and  $\Gamma_8$  bands and then removing the  $L1$  sub-band which splits off. The remaining basis has four orbitals: the first two are  $|s, S_z = 1/2\rangle$ ,  $|p, S_z = 1/2\rangle$ , and the last two have  $S_z$  reversed.<sup>27</sup> The BHZ model's momentum representation is:

$$\begin{aligned} \mathcal{H} &= \begin{bmatrix} h(\vec{k}) & 0 \\ 0 & h^*(-\vec{k}) \end{bmatrix} \\ h(\vec{k}) &= (A/a)\sigma_x \sin(k_x a) + (A/a)\sigma_y \sin(k_y a) + M\sigma_z \\ &\quad + 2(\sigma_z B/a^2 + I D/a^2)(2 - \cos(k_x a) - \cos(k_y a)) \\ D &= 512 \text{ meV nm}^2, B = 686 \text{ meV nm}^2, \\ A &= 364.5 \text{ meV nm}, a = 5 \text{ nm}, M = -10 \text{ meV} \end{aligned} \quad (1)$$

$\sigma_{x,y,z}$  are the Pauli matrices, and the sines and cosines in the Hamiltonian ensure the correct topological band structure.  $a = 5 \text{ nm}$  is the lattice spacing. The penetration depth of the in-gap surface states is always less than  $5a = 25 \text{ nm}$ , which gives us good control of finite size effects when calculating the conductance in strips of width  $3a$  to  $28a$ . Finite size effects are practically absent in our other calculations, where we have checked that changing the system size from  $200a \times 200a$  to  $400a \times 400a$  makes very little difference in our results. The mass  $M$  can be tuned by changing the sample thickness, and we choose a negative mass  $M = -10 \text{ meV}$  so that there is a band

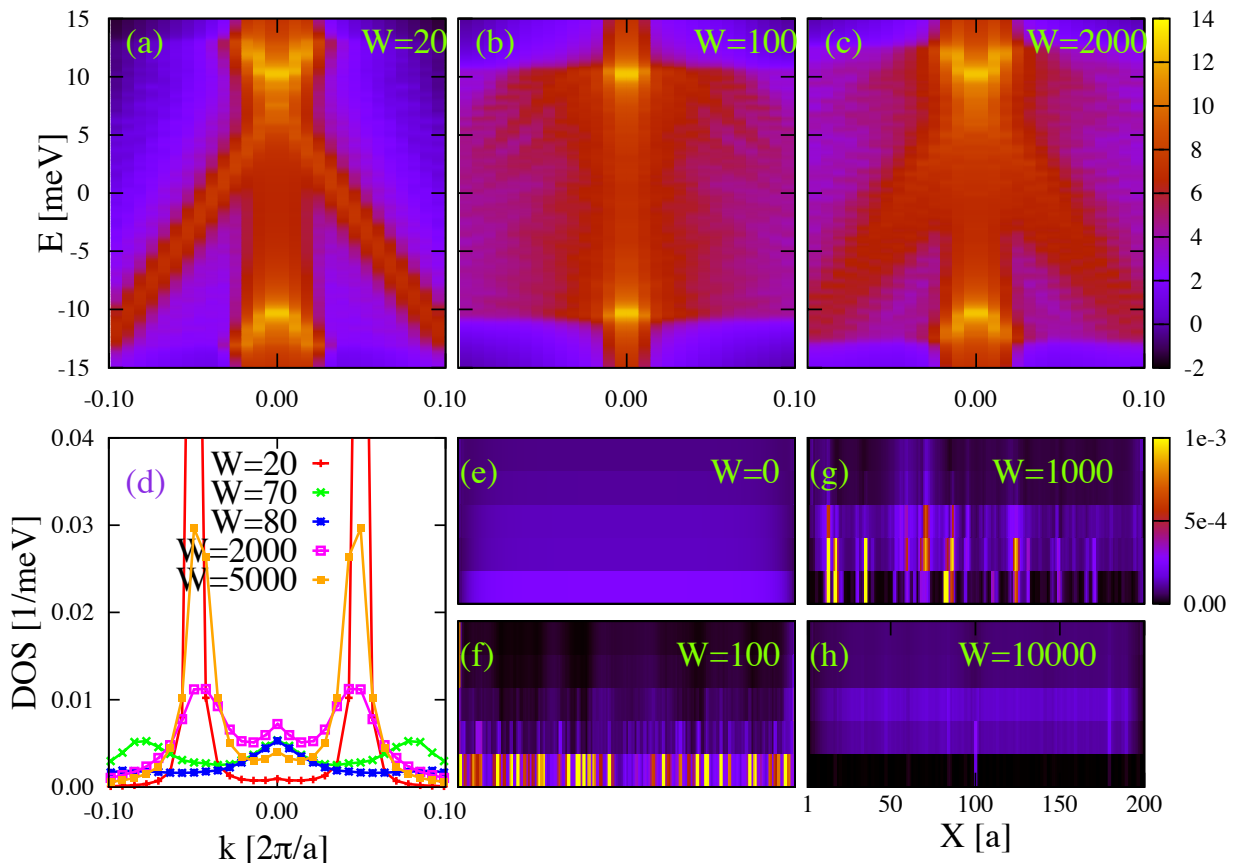


FIG. 1: (Color online.) Effects of disorder on the spectral density  $A(\vec{k}, E)$  and typical surface states. Panes a, b, and c show the spectral density as a function of both energy  $E$  and wave-number  $k$  at small disorder ( $W = 20$  meV), intermediate disorder ( $W = 100$  meV), and large disorder ( $W = 2000$  meV). The Dirac cone's two lines are clearly visible at small disorder and large disorder, but disappear in a range starting at  $W = 80$  meV and extending to near  $W = 2000$  meV. Pane d shows the averaged spectral density on a cross section  $E = -2.5$  meV; the Dirac cone is signaled by two symmetric peaks and is absent in a range starting at  $W = 80$  meV. Panes e-h show typical surface states at four representative disorder strengths. In all cases they are extended and conducting, but at  $W = 100, 1000$  meV they lose their plane wave character and therefore are not visible in the spectral density.

inversion. This mass can be produced by fabricating a quantum well with a thickness of  $\sim 70$  Å.<sup>28</sup> With this mass the bulk exhibits a band gap in the interval  $[-10, 10]$  meV, and the Dirac point lies near 8 meV. The valence band extends over  $[-62, -10]$  meV, and the conduction band extends over  $[10, 373]$  meV. The bulk bandwidths of 52 meV, 363 meV are important - we will show that they set the scale of the disorder's effects on the Dirac dispersion.

The BHZ model conserves the  $S_z$  component of the spin, which is protected by bulk inversion symmetry. This symmetry can be broken by a quantum well or gate electrode<sup>28</sup>, and also can be broken by disorder. We introduce disorder on the outer two layers ( $2a = 10$  nm) of the TI, and this disorder is white noise without any correlation between sites. We follow several papers<sup>29–31</sup> which preserved the  $S_z$  symmetry and used nonmagnetic on-site disorder randomly distributed in the interval  $[-W/2, W/2]$ , where  $W$  is the disorder strength. With this disorder the BHZ model factorizes into two indepen-

dent  $2 \times 2$  Hamiltonians which are time-reversal counterparts of each other, and its universality class changes from symplectic to unitary. Although this change is pertinent to disorder effects in the bulk<sup>31–35</sup>, it does not affect the present paper's results on surface disorder with a clean bulk. Here the conducting states in the gap are edge states controlled a  $2 \times 2$  effective Hamiltonian whose symmetry class is independent of the BHZ model's  $S_z$  symmetry. All of our calculations of the conductance, eigenvectors, and eigenvalues concern themselves only with the  $S_z = 1/2$  sector, which is a time-reversed copy of the  $S_z = -1/2$  sector.

With the exception of our conductance data, all of our numerical results come from a leads-free geometry. However for the conductance we use a strip with two attached clean semi-infinite leads that have widths equal to the width of the strip itself. We evaluate the conductance using the Caroli formula<sup>36,37</sup>  $G = -\frac{e^2}{h} \text{Tr}((\Sigma_L^r - \Sigma_L^a)G_{LR}^r(\Sigma_R^r - \Sigma_R^a)G_{RL}^a)$ , where  $G^a, G^r$  are the advanced

and retarded Green's functions connecting the left and right leads and  $\Sigma_{L,R}$  are the self-energies of the leads. We evaluate the lead self-energies using the well-known iterative technique developed by Lopez Sancho et al.<sup>38</sup>

### III. RESULTS

Panes a-d of Figure 1 summarize the spectral density - the square  $A(\vec{k}, E) = \sum_n \delta(E - E_n) |\langle \vec{k} | \psi_n \rangle|^2$  of the eigenstates  $|\psi_n\rangle$ , resolved in momentum space. This quantity is very attractive because in pure samples it shows a clear X-shaped signal marking the surface state Dirac cone, and because in 3-D TIs it may be measured with ARPES. Such measurements have been very popular both for proving that particular materials are topological insulators and for diagnostic evaluations of individual experimental samples. In panes a-c of Fig. 1 we report the spectral density in the band gap of a single 2-D  $400a \times 400a$  sample, using a logarithmic color scale. Pane a shows the spectral density of a weakly disordered sample ( $W = 20$  meV), which is substantially the same as the density of a disorder-free sample. The two straight lines of the Dirac cone are very clear, and the Dirac point lies near 8 meV. Above 10 meV and below  $-10$  meV the bulk valence and conduction bands are visible as very bright curves. In pane b we increase the disorder strength to  $W = 100$  meV and observe that the Dirac dispersion is no longer visible while the bulk bands remain unchanged. Lastly pane c shows that when the disorder strength is far larger than the band width ( $W = 2000$  meV vs. 363 meV) the surface states again manifest themselves in a clearly visible linear Dirac dispersion. Pane d tells the same story with more precision by focusing on a cross-section of  $A(\vec{k}, E)$  at  $E = -2.5$  meV and averaging over 1000  $200a \times 200a$  samples. The data for small disorder ( $W = 20, 70$  meV) show two peaks at  $|\vec{k}| = |E - E_0|/\hbar v_F$  corresponding to the two branches of the Dirac cone. The peaks disappear at  $W = 80$  meV and reappear near  $W = 2000$  meV. These results agree completely with Schubert et al's study of the spectral density in 3-D TIs<sup>23</sup> which found that the Dirac cone is absent from the spectral density at intermediate disorders but reappears at large disorders. Our results also are consistent with several experimental ARPES observations of a weakened Dirac cone in 3-D TIs with surface disorder.<sup>10-12</sup>

To understand the fate of the surface states we calculate individual surface states at four representative disorder strengths and show their probability distributions  $|\psi(\vec{x})|^2$  in panes e - h of Figure 1. We plot the lower 5 layers of  $200a \times 200a$  samples, choose  $E = 7.5$  meV, and employ a linear color scale. In all cases the great majority of surface states remain extended along the entire perimeter of the TI sample and strongly avoid the sample's interior. By collecting large numbers of surface states we have found a small sub-population of very localized states in the gap, but these states are a small

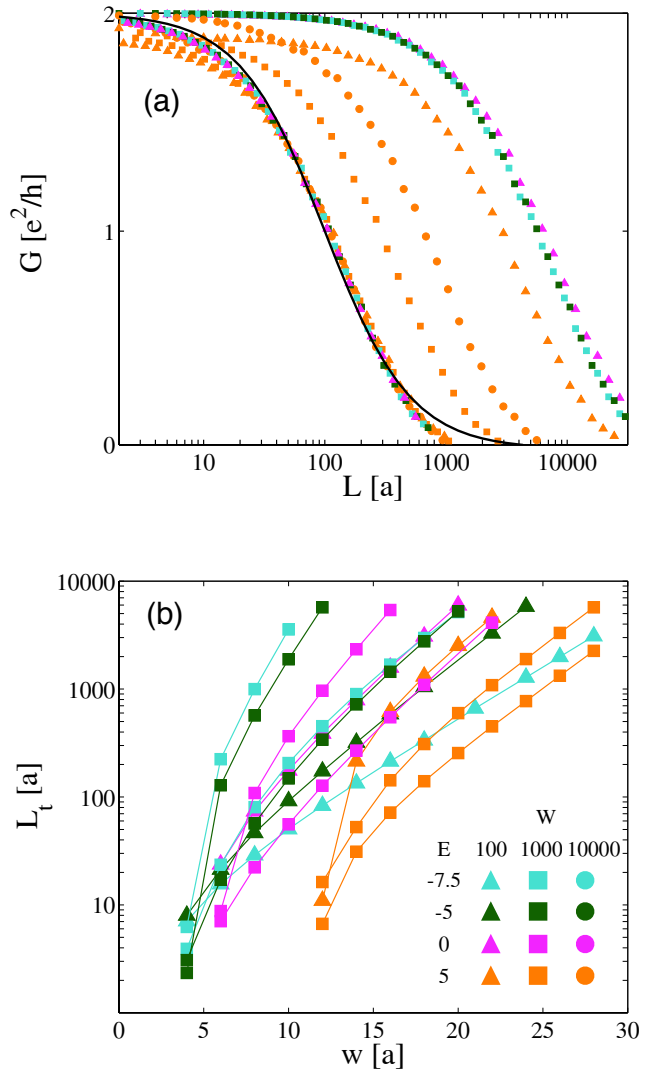


FIG. 2: (Color online.) Robust topological protection of surface conduction, limited only by tunneling through the bulk. Pane a shows how we determine the tunneling length  $L_t$ . The average conductance follows a universal curve, which is shown in the left-most curve. The thin black line shows a best fit with the hyperbolic tangent function. We determine the tunneling length  $L_t$  by finding the point where the average conductance is equal to 1. Pane b shows  $L_t$  as a function of strip width  $w$  for several Fermi energies and disorder strengths, including  $W = 10^4$  meV which far exceeds the band width. Each curve converges rapidly to a straight line, proving that the tunneling length becomes exponentially large when the strip is widened, and that surface conduction is topologically protected in wide strips.

fraction of the total.<sup>40</sup> Pane e shows a surface state at zero disorder. It is a plane wave; its density is constant along the sample edge. Likewise pane h shows that at large disorder ( $W = 10^4$  meV) the surface states shift inward into the sample, avoiding the outer two disordered layers, and therefore have a smooth plane wave character. However at intermediate disorders  $W = 100, 1000$  meV the surface states are strongly affected by the disorder.

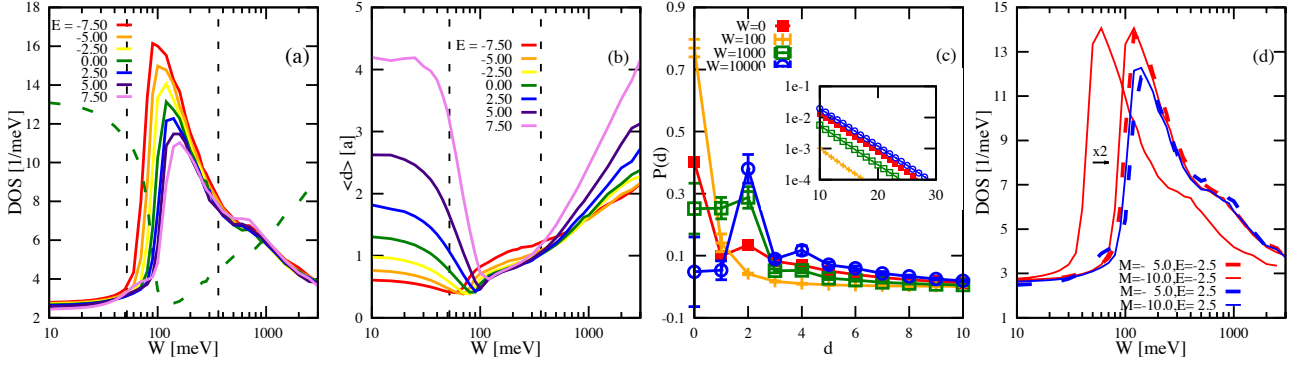


FIG. 3: (Color online.) The resonance between disorder and the bulk band which is responsible for disrupting the Dirac cone. Pane a shows the density of states at seven Fermi levels inside the band gap. A clear resonance is visible at the characteristic bulk band widths [52, 363] meV, which are marked with vertical dashed lines. The green dashed line plots the profile of the Fermi velocity at  $E = 0$  meV, which is inversely proportional to the DOS. The units are arbitrary. Pane b shows the average distance from the edge ( $d$ ), while pane c plots the probability  $P(d)$  as a function of distance from the edge. Both panes show that in the resonant region the surface states are pulled into the disordered layers. The inset in pane c shows that deep inside the bulk the surface states are controlled by the penetration length plus a shift caused by the resonance. Pane d shows the density of states when the band gap lies in the interval  $[-10, 10]$  meV, or instead in the interval  $[-5, 5]$  meV. The curve far to the left shows where the  $[-5, 5]$  meV DOS curve would be if the resonance were controlled by the band gap instead of the band width.

der and become very inhomogeneous. This explains the absence of a Dirac cone structure in the spectral density. Extended surface states are present regardless of the disorder strength, but at  $W = 100, 1000$  meV they are not plane waves and therefore have no structure in momentum space.

Although the surface states are no longer visible in the spectral density, they remain topologically protected and in wide strips the conductance remains forever quantized. In Figure 2 we calculate the conductance in long TI strips and show that the only mechanism which destroys conduction is tunneling across the strips. In these conductance calculations we introduce disorder only in the outermost layer of the TI. The tunneling occurs at a characteristic strip length  $L_t$  which can be measured by calculating the average conductance as a function of strip length  $L$ , as seen in Fig. 2a. We calculated this function at a variety of disorder strengths and Fermi energies, averaging over 3000 disorder realizations and keeping the strip width fixed at  $w = 20a$ . In each case (except for small strip widths) the average conductance follows an identical curve, as shown in the left-most curve where we have shifted all the data to coincide with each other. The universal curve is nearly linear in the interval  $G = [0.4, 1.4]$  and is fairly similar to the hyperbolic tangent, which is marked by a thin black line. This makes us confident that we can reliably calculate the tunneling length scale  $L_t$  by determining the value of  $L$  which satisfies  $G(L) = 1$ . In pane b we plot  $L_t$  as a function of strip width  $w$ . Each curve is determined by varying the strip width while keeping the disorder strength and Fermi level constant. We explore the bulk band gap between  $[-10, 10]$  meV by calculating four Fermi energies  $E = -7.5, -5, 0, 5$  meV. We also explore three disorder

strengths  $W = 10^2, 10^3, 10^4$  which all far exceed the bulk band gap, and the last of these far exceeds the band width. At small strip widths the curves show some bending caused by finite size effects. Nonetheless each curve quickly converges to a straight line; the tunneling length  $L_t$  is proportional to  $L_t \propto e^w$  and is exponentially large in a wide strip. This proves that the conductance remains forever quantized in an infinitely wide strip; surface conduction is robustly protected regardless of the disorder strength. The surface states inside the bulk band gap remain always extended and conducting.

Lastly we study the physics which disrupts the Dirac cone signal in the spectral density, which is a resonance between the disorder potential and the bulk bands at the characteristic bulk band widths [52, 363] meV. Pane a of Figure 3 reports the density of states (DOS)'s dependence on disorder, which we obtained by collecting eigenvalue-eigenstate pairs near specified Fermi energies  $E = -7.5, \dots, 7.5$  meV and averaging over 100 disorder realizations. First we note that the DOS (and all other observables) evolves continuously; the absent Dirac cone can not be explained by an absence of surface states. Inside the interval  $E = [52, 363]$  meV the DOS first grows sharply and then begins to decay more slowly. The peak over base ratio of this resonance is about 5.8. On the left shoulder of the resonance we see a spread between the DOS curves measured at different Fermi energies, indicating that the density of states increases first near the valence band and soon after at higher Fermi energies. The valence band has a much smaller bandwidth, so it is natural that the left shoulder of the resonance has a predominantly valence band character. Outside of the resonance the DOS tends toward its disorder-free value. Except for in the resonance's left shoulder which is rela-

tively small, the DOS is independent of the Fermi energy, as expected of Dirac states on the edge of a 2-D TI.

Panes b and c of Figure 3 show that the resonance pulls the edge states into the disordered sites on the boundary of the TI. Two authors have already briefly discussed this behavior at a qualitative level<sup>30,39</sup>; here we measure it quantitatively and establish its dependence on the disorder strength and the Fermi energy. Pane b plots the average distance from the edge - the expectation value  $\langle d \rangle = \int d^2\vec{x} |\psi(\vec{x})|^2 d(\vec{x})$  of the distance  $d(\vec{x})$  to the nearest edge. Again we have averaged over 100 disorder realizations. Outside of the resonant interval [52, 363] meV  $\langle d \rangle$  depends strongly on the Fermi level and is maximized near the Dirac point  $E = 8$  meV. This behavior is linked to the penetration depth which is also energy dependent, and contrasts strongly with the resonant interval where  $\langle d \rangle$  is practically independent of energy. Inside the resonance the state's position is determined by disorder and not by the penetration depth.  $\langle d \rangle$  is strongly reduced to about one lattice unit; the surface states reside almost entirely in the outer two layers where we have introduced disorder. We see this more precisely in pane c, which plots the probability  $P(d) = \int d^2\vec{x} |\psi(\vec{x})|^2 \delta(d - d(\vec{x}))$  that the state is located on layer  $d$ . We examine four disorder strengths, average over  $10^4$  disorder realizations, and keep the Fermi energy fixed at 5 meV. Inside the resonant interval  $P(d)$  becomes strongly concentrated on the outer two layers; the probability on the outer layer  $P(0)$  almost doubles from the pure case to  $W = 100$  meV. As the disorder is increased beyond the band width the surface states are expelled from the disordered layers which are no longer part of the TI because their band structure is overwhelmed by disorder. The surface states concentrate at the boundary between the disordered layers and the clean layers which retain their TI band structure. The inset shows that deep inside the TI  $P(d)$  is always controlled by the penetration depth and decays exponentially. Here the only effect of disorder is to shift  $P(d)$  first inward at intermediate disorder strengths and then outward at large disorder. This effect is similar to the phase shifts found in the theory of scattering events.

The above discussion suggests that the bulk band width not the bulk band gap controls the energy scales at which Dirac cone is protected or destroyed. This result contrasts with at least one previous paper<sup>23</sup> which expected that the Dirac cone is protected by the bulk band gap. Therefore we checked this question directly by changing the gap to  $[-5, 5]$  meV, in contrast to the rest of our calculations where we set the gap to  $[-10, 10]$  meV. We recomputed the DOS, the average distance from the edge, and the participation ratio. If the bulk gap were the controlling factor then a 0.5 reduction of the band

gap should shift all observables to smaller disorders, i.e.  $W \rightarrow W/2$ . Pane d of Figure 3 shows where the DOS would shift to if the bulk gap were the controlling scale. We observe that the DOS (and other observables) shift slightly in the opposite direction. This confirms that the Dirac cone is topologically protected from surface disorder by the bulk band width not the bulk band gap, and agrees with the well-established fact that bulk disorder destroys the topologically protected surface band only when it reaches the scale of the bulk band.<sup>21,31</sup>

#### IV. DISCUSSION

The resonance which we have observed in the DOS is caused by resonances between individual disordered sites and the edge states. As an electron moves along the edge of the TI it from time to time becomes almost trapped at a particular site and dwells there for a while before continuing its journey. This trapping is unable to destroy the edge state but it does introduce both a phase shift and a localized increase in the surface state's probability density. This destroys both the edge state's plane wave character and the Dirac cone. The trapping naturally also decreases the Fermi velocity of the edge states. In pane a of Figure 3 we have plotted the profile of the Fermi velocity, which can be easily computed because both dimensional analysis and the Dirac relation  $E = v_F \hbar |k|$  indicate that it is inversely proportional to the density of states. At its peak the resonance divides the (average) Fermi velocity by 5.8 and as a result multiplies the DOS by the same number.

In synthesis, our results suggest that surface conduction always remains controlled by an effective linear Dirac Hamiltonian, albeit renormalized by disorder. The states in the bulk gap remain very close to the TI's boundary, and we have found that the surface states' energy levels always remain evenly spaced. These facts argue that the in-gap states are described well by a surface Hamiltonian. The robust  $2G_0$  conductance indicates that the surface states never backscatter, which is consistent with spin-momentum locking on a Dirac cone. Moreover their DOS is generally independent of energy as expected of a 2-D Dirac cone. We conclude that disorder renormalizes the surface states but does not alter their Dirac physics. They are well described by a linear Dirac Hamiltonian with renormalized parameters. The main effects of surface disorder are to reduce the Fermi velocity, increase the DOS, and first pull the states into the disordered region and later (at very strong disorder) expel them into the clean bulk.

---

\* Electronic address: vincent@sacksteder.com

<sup>1</sup> C. L. Kane and E. J. Mele, Physical Review Letters **95**,

226801 (2005).

<sup>2</sup> H. Zhang, C.-X. Liu, X.-L. Qi, X. Dai, Z. Fang, and S.-C.

- Zhang, *Nature Physics* **5**, 438 (2009).
- <sup>3</sup> M. Z. Hasan and C. L. Kane, *Reviews of Modern Physics* **82**, 3045 (2010).
  - <sup>4</sup> Y. Q. Li, K. H. Wu, J. R. Shi, and X. C. Xie, *Front. Phys.* **7**, 165 (2012).
  - <sup>5</sup> D. Culcer, *Physica E* **44**, 860 (2012).
  - <sup>6</sup> J. G. Analytis, J.-H. Chu, Y. Chen, F. Corredor, R. D. McDonald, Z. X. Shen, and I. R. Fisher, *Physical Review B* **81**, 205407 (2010).
  - <sup>7</sup> M. Brahlek, Y. S. Kim, N. Bansal, E. Edrey, and S. Oh, *Applied Physics Letters* **99**, 012109 (2011).
  - <sup>8</sup> R. V. Aguilar, A. V. Stier, W. Liu, L. S. Bilbro, D. K. George, N. Bansal, L. Wu, J. Cerne, A. G. Markelz, S. Oh, et al., *Physical Review Letters* **108**, 087403 (2012).
  - <sup>9</sup> O. E. Tereshchenko, K. A. Kokh, V. V. Atuchin, K. N. Romanyuk, S. V. Makarenko, V. A. Golyashov, A. S. Kozhukhov, I. P. Prosvirin, and A. A. Shklyaev, *JETP Letters* **94**, 465 (2011).
  - <sup>10</sup> D. Hsieh, Y. Xia, D. Qian, L. Wray, J. H. Dil, F. Meier, J. Osterwalder, L. Patthey, J. G. Checkelsky, N. P. Ong, et al., *Nature* **460**, 1101 (2009).
  - <sup>11</sup> H. J. Noh, J. Jeong, E. J. Cho, H. K. Lee, and H. D. Kim, *EPL* **96**, 47002 (2011).
  - <sup>12</sup> Z. K. Liu, Y. L. Chen, J. G. Analytis, S. K. Mo, D. H. Lu, R. G. Moore, I. R. Fisher, Z. Hussain, and Z. X. Shen, *Physica E* **44**, 891 (2012).
  - <sup>13</sup> M. Lang, L. He, F. Xiu, X. Yu, J. Tang, Y. Wang, X. Kou, W. Jiang, A. V. Fedorov, and K. L. Wang, *ACS Nano* **6**, 295 (2011).
  - <sup>14</sup> J. Chen, H. J. Qin, F. Yang, J. Liu, T. Guan, F. M. Qu, G. H. Zhang, J. R. Shi, X. C. Xie, C. L. Yang, et al., *Physical Review Letters* **105**, 176602 (2010).
  - <sup>15</sup> D. Kong, J. J. Cha, K. Lai, H. Peng, J. G. Analytis, S. Meister, Y. Chen, H.-J. Zhang, I. R. Fisher, Z.-X. Shen, et al., *ACS Nano* **5**, 4698 (2011).
  - <sup>16</sup> B. A. Bernevig, T. L. Hughes, and S.-C. Zhang, *Science* **314**, 1757 (2006).
  - <sup>17</sup> B. Buttner, C. X. Liu, G. Tkachov, E. G. Novik, C. Brune, H. Buhmann, E. M. Hankiewicz, P. Recher, B. Trauzettel, S. C. Zhang, et al., *Nature Physics* **7**, 418 (2011).
  - <sup>18</sup> Z. D. Kvon, S. N. Danilov, D. A. Kozlov, C. Zoth, N. N. Mikhailov, S. A. Dvoretiskii, and S. D. Ganichev, *JETP Letters* **94**, 816 (2011).
  - <sup>19</sup> D. Pesin and L. Balents, *Nature Physics* **6**, 376 (2010).
  - <sup>20</sup> L. Chen, Q. Liu, X. Lin, X. Zhang, and X. Jiang, *New Journal of Physics* **14**, 043028 (2012).
  - <sup>21</sup> D. Xu, J. Qi, J. Liu, V. S. IV, X. C. Xie, and H. Jiang, *Physical Review B* **85**, 195140 (2012).
  - <sup>22</sup> Z. Ringel, Y. E. Kraus, and A. Stern, *Physical Review B* **86**, 045102 (2012).
  - <sup>23</sup> G. Schubert, H. Fehske, L. Fritz, and M. Vojta, *Physical Review B* **85**, 201105 (2012).
  - <sup>24</sup> S. Hikami, A. I. Larkin, and Y. Nagaoka, *Prog. Theor. Phys. Progress Letters* **63**, 707 (1980).
  - <sup>25</sup> J. H. Bardarson, J. Tworzydło, P. W. Brouwer, and C. W. J. Beenakker, *Physical Review Letters* **99**, 106801 (2007).
  - <sup>26</sup> K. Nomura, M. Koshino, and S. Ryu, *Physical Review Letters* **99**, 146806 (2007).
  - <sup>27</sup> Y. Y. Zhang, R. L. Chu, F. C. Zhang, and S. Q. Shen, *Physical Review B* **85**, 035107 (2012).
  - <sup>28</sup> D. G. Rothe, R. W. Reithaler, C. X. Liu, L. W. Molenkamp, S. C. Zhang, and E. M. Hankiewicz, *New Journal of Physics* **12**, 065012 (2010).
  - <sup>29</sup> J. Li, R.-L. Chu, J. K. Jain, and S.-Q. Shen, *Physical Review Letters* **102**, 136806 (2009).
  - <sup>30</sup> H. Jiang, L. Wang, Q. F. Sun, and X. C. Xie, *Physical Review B* **80**, 165316 (2009).
  - <sup>31</sup> C. W. Groth, M. Wimmer, A. R. Akhmerov, J. Tworzydło, and C. W. J. Beenakker, *Physical Review Letters* **103**, 196805 (2009).
  - <sup>32</sup> E. Prodan, *Physical Review B* **83**, 195119 (2011).
  - <sup>33</sup> M. Onoda, Y. Avishai, and N. Nagaosa, *Physics Review Letters* **98**, 076802 (2007).
  - <sup>34</sup> H. Obuse, A. Furusaki, S. Ryu, and C. Mudry, *Physics Review B* **76**, 075301 (2007).
  - <sup>35</sup> A. Yamakage, K. Nomura, K.-I. Imura, and Y. Kuramoto, *Journal of the Physical Society of Japan* **80**, 053703 (2011).
  - <sup>36</sup> C. Caroli, R. Combescot, P. Nozieres, and D. Saint-James, *Journal of Physics C* **4**, 916 (1971).
  - <sup>37</sup> Y. Meir and N. S. Wingreen, *Physics Review Letters* **68**, 2512 (1992).
  - <sup>38</sup> M. P. L. Sancho, J. M. L. Sancho, and J. Rubio, *Journal of Physics F: Metal Physics* **15**, 851 (1985).
  - <sup>39</sup> R.-L. Chu, J. Li, J. K. Jain, and S.-Q. Shen, *Physical Review B* **80**, 081102(R) (2009).
  - <sup>40</sup> In  $200a \times 200a$  samples at  $E = 5$  meV with  $W = 10^3$  meV  $11.9 \pm 1.1$  percent of the states have participation ratios (PRs) less than 50, and  $2.4 \pm 0.5$  percent have PRs less than 10. At  $W = 10^4$  meV these proportions are  $5.9 \pm 0.8$  and  $4.9 \pm 0.7$  percent.